Functional impact of a deep intronic variant in the *RPS19* gene detected in a case of Diamond-Blackfan anemia syndrome

Diamond-Blackfan anemia syndrome (DBAS) is a rare inherited disorder characterized by pure red cell aplasia, usually presenting in infancy.[1] It can also be associated with a variety of malformations and a high risk of developing malignancy. To date, causative mutations for DBAS have been found in more than 20 ribosomal protein (RP) genes,[1-3] *TSR2*,[4] *HEATR3*,[5] *GATA1*,[6] and *TP53*,[7] but remain unclear in approximately 20% of DBAS cases.[3] Here, we report the identification of a deep intronic *RPS19* variant causing aberrant splicing in a patient with DBAS that was revealed by whole genome sequencing (WGS) analysis.

A boy was born at full term with bilateral polydactyly of the thumbs. He had no family history of anemia. At one month old, he presented with pallor and tachycardia, and peripheral blood analysis showed red blood cell (RBC) count 0.64x10^{12}/L, hemoglobin (Hb) 2.4 g/dL, mean corpuscular volume 107.8 fL, reticulocytes 0.2%, white blood cell count 4.10x10^{9}/L, platelets 258x10^{9}/L, and fetal Hb 16.4%. Bone marrow aspiration revealed hypercellularity, with 0% erythroid cells. His erythrocyte adenosine deaminase activity (eADA) and glutathione (GSH) levels were 1.11 IU/g Hb (normal range 0.46-1.50 IU/g Hb) and 122 mg/dL RBC (normal range 62.4-98.9 mg/dL RBC), respectively, suggesting a DBA pattern using a previously reported formula.[8] After diagnosis, he became transfusion dependent.

This study was conducted with the approval of the Ethics Committees of Hirosaki University and the National Institute of Global Health and Medicine, Japan, and peripheral blood samples were collected with informed consent. All experiments were performed in accordance with the principles of the Declaration of Helsinki.

Whole genome sequencing was performed on the Illumina NovaSeq 6000 platform (Illumina) with 150-base pair (bp) paired-end reads. The target sequencing depth was approximately 30× for each individual. Quality-filtered reads were aligned to the human reference genome (GRCh38/hg38) using BWA-MEM (version 0.7.17). Single-nucleotide variants (SNV) and small insertions/deletions (indels) were identified using GATK HaplotypeCaller (version 4.1.0.0), following the GATK Best Practices workflow. Structural variants, including deletions, duplications, inversions, and translocations, were detected using Manta (version 1.6.0). Variant annotation was performed using ANNOVAR and InterVar for SNV and small indels, and the Ensembl Variant Effect Predictor for structural variants.

Functional impacts were assessed using LOFTEE (version 1.0) for loss-of-function prediction, SpliceAI (version 1.3.1) for splicing prediction, and CADD (version 1.6) for deleteriousness scoring. We did not detect any mutations that could cause DBAS in coding regions, but SpliceAI predicted a splice abnormality to a *de novo* variant in the third intron of *RPS19* (hg38:chr19:41862119A>G, NM_001022:c.172+907A>G) (Figure 1A, B). This variant was not present in the 1000 Genomes Project, gnomAD or the Japanese Multi Omics Reference Panel 61KJPN database. Given the phenotype of the patient, it was considered potentially pathogenic. Barrio *et al*. had previously reported the variant as novel-20 (rs61761229) in a paper on *RPS19* targeted resequencing using DBA and transient erythroblastopenia in childhood (TEC) samples,[9] but it has not yet been identified as a disease-causing mutation or characterized functionally. Upon reviewing the details in the web version of SpliceAI (https://spliceailookup.broadinstitute.org), we found that the variant would create a novel donor splice site one base upstream of the variant (Donor Gain Δ score 0.83; values above 0.8 are high precision), and that the AG sequence of the original cryptic splicing site upstream of the variant (Acceptor Gain Δ score: 0.81) would result in an acceptor splice site 152 bp upstream (Figure 1A).

Reverse transcription polymerase chain reaction (RT-PCR) detected a transcript approximately 150 bp longer than the normal product exclusively in the patient, and only in trace amounts; no such transcript was observed in either parent (Figure 1C). Subsequent sequencing of the RT-PCR product identified a 152-bp cryptic exon inserted between the third and fourth exons, consistent with the prediction by SpliceAI (Figure 1D). The extremely low abundance of this aberrant transcript is likely due to nonsense-mediated mRNA decay (NMD),[10] triggered by a premature termination codon (PTC) within the cryptic exon (Figure 1A, E).

To evaluate the impact of this variant on splicing, we performed genome editing using the erythroid cell line HUDEP-2.[11] In practice, we first created HUDEP-Cas9 cells, which constitutively express Cas9 to enhance genome editing efficiency, and performed the experiment. The methods used have been described previously.[12] A>C corresponds to the control of this experiment and A>G is a single-base substitution identical to the variant in the patient. Both were efficiently incorporated into the cells (Figure 2A). Subsequent RT-PCR confirmed that the *RPS19* transcript pattern in the patient was recapitulated in HUDEP-2 Cas9 cells (Figure 2B). In the quantitative RT-PCR (qRT-PCR), a decrease in *RPS19* mRNA was observed in the A>G genome-edited cells (fold change: 0.58 ± 0.09),

while the transcript levels of *RPL5* and *RPL11* were little changed (Figure 2C). This suggests that the reduction in *RPS19* mRNA caused by this A>G genome editing is specific to this gene.

We hypothesized that if the reduction in *RPS19* mRNA levels observed in A>G genome-edited cells was due to

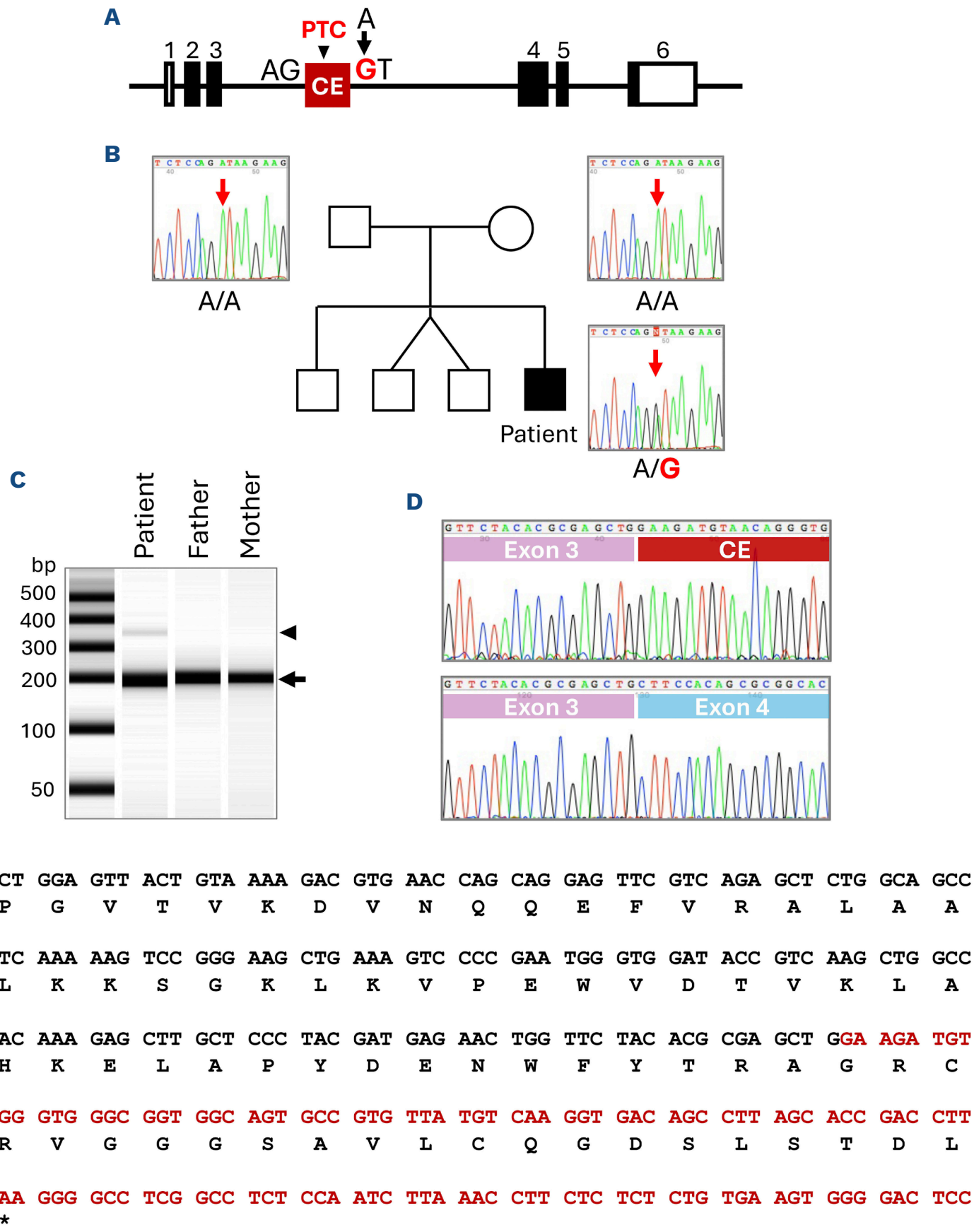

Figure 1. Sequence of the *RPS19* intronic variant and splice aberrations in the patient. (A) Schematic diagram of *RPS19* gene structure and location of the variant. Black and white boxes indicate coding and non-coding exons, respectively. Arrow indicates location of a single nucleotide substitution A>G in this patient. Red box shows cryptic exon (CE) predicted to be formed by presence of this variant; arrowhead indicates a premature termination codon (PTC) is indicated. (B) Pedigree of the patient and Sanger sequencing results of the variant region using genomic DNA. Red arrows indicate the position of nucleotide substitution c.172+907A>G. (C) Reverse transcription polymerase chain reaction (RT-PCR) analysis using the primer set located on the second and fourth exons of the *RPS19* gene. Arrow indicates fragments corresponding to normal transcripts; arrowhead indicates fragments corresponding to transcripts containing the cryptic exon. (D) Sanger sequencing of *RPS19* RT-PCR products. Electropherograms of the boundary between the third exon and the adjacent exon are shown. (Top) Transcript containing the cryptic exon. (Bottom) Normal transcript. (E) *RPS19* cDNA coding sequence with the cryptic exon. First line shows the *RPS19* cDNA sequence; second line shows the corresponding amino acid. cDNA sequence of the cryptic exon region in red. The protein from this transcript is p.Ala58Glyfs*25.

aberrant splicing induced by the A>G variant, blocking the splice site of the cryptic exon could restore normal expression of *RPS19* mRNA. Therefore, we transfected a S19 int3 morpholino antisense oligonucleotide (MO)[13] targeting the splicing donor site of the cryptic exon containing the A>G substitution into genome-edited cells. As a result, qRT-PCR showed that *RPS19* mRNA levels were restored according to the concentration of S19 int3 MO in A>G genome-edited cells, while no change was observed in A>C genome-edited cells (Figure 2D, left). Conversely, transcripts containing

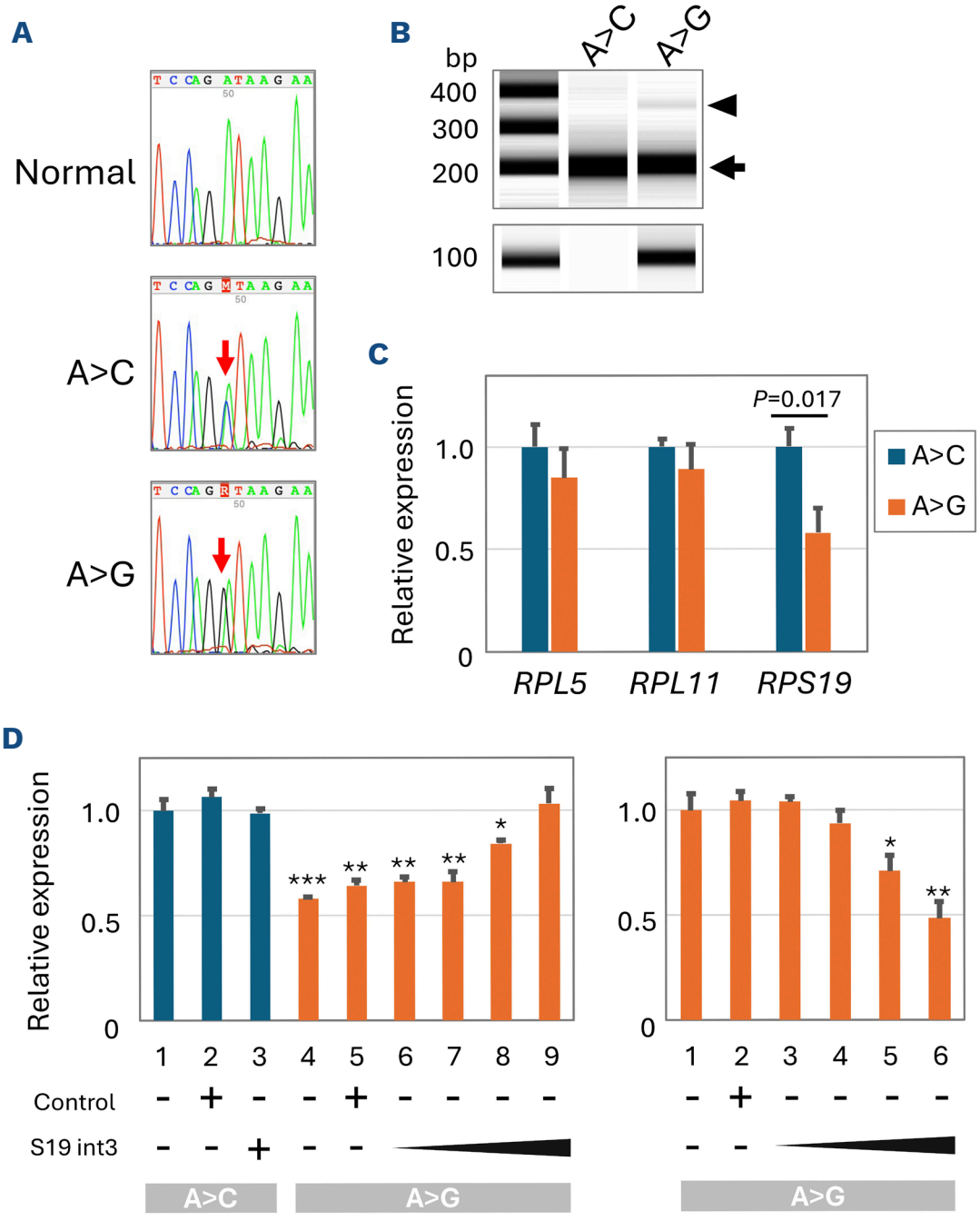

Figure 2. Functional analysis of the variant by genome editing. (A) Confirmation of genome editing of *RPS19* intronic variant in HUDEP-2 Cas9 cells. Genomic DNA extracted from samples four days after genome editing was subjected to Sanger sequencing. (B) Real-time polymerase chain reaction (RT-PCR) analysis using RNA extracted from samples four days after genome editing. (Top) The same primer pair used in Figure 1C was used here. Arrow indicates fragments corresponding to normal transcripts; arrowhead indicates fragments corresponding to transcripts containing the cryptic exon. (Bottom) To specifically amplify transcripts containing the cryptic exon, nested PCR was performed using samples from the above panel as templates. The primer pairs used were in the third exon and the cryptic exon. (C) Quantitative RT-PCR (qRT-PCR) analysis of *RPS19* genome-edited cells at day 14. The total *RPS19* transcript was quantified using the same primer pair located on the fifth and sixth exons of the *RPS19* gene. The vertical axis represents a relative value with each value of A>C cells set at 1. Results are averages of 3 independent experiments. Error bars represent standard deviation. *P* value by two-sided *t* test. (D) Splicing inhibition of the cryptic exon by Morpholino antisense oligonucleotide (MO). *RPS19* genome-edited day 14 cells that had been frozen were thawed and transfected with MO two days later. Samples were collected 48 hours after transfection and qRT-PCR was performed. + and – symbols at the bottom of the graphs indicate whether control MO or S19 int3 MO was used. The target sequence of S19 int3 MO is 5'-GCTTCCCACCTACTTCTTACCTGGA-3', the underlined nucleotide indicates the antisense base of the patient's variant. + indicates addition of MO at 10 μM. In lanes 6 to 9 of the left graph and lanes 3 to 6 of the right graph, MO was increased to 0.05, 0.5, 5 and 10 μM. (Left) The total *RPS19* transcript was quantified using the same primer pair as in Figure 2C. The vertical axis represents a relative value of A>C cells with control MO 10 μM (lane 2) set at 1. (Right) Transcripts containing the cryptic exon were specifically quantified and the primer pair used was the same as in Figure 2B, bottom. The vertical axis represents a relative value of A>G cells with control MO 10 μM (lane 2) set at 1. Results are averages of 3 independent experiments. Error bars represent standard deviation. Two-sided *t* tests compared to lane 2 values for both graphs, respectively. **P*<0.05, ***P*<0.01, ****P*<0.001.

the cryptic exon in A>G genome-edited cells were reduced according to the concentration of S19 int3 MO (Figure 2D, right). Thus, the reduction in *RPS19* mRNA levels in the *RPS19* A>G genome-edited cells was confirmed to be due to the A>G variant causing aberrant splicing. These results suggest that this deep intronic variant causes *RPS19* haploinsufficiency, which would lead to DBA.

Identification of responsible genes for inherited disease is crucial for appropriate diagnosis, and for selecting and developing treatment. In recent years, WGS has come into use, but there are still cases where the causative gene of DBAS cannot be identified. This indicates that the genetic abnormality that affects DBAS may not be restricted to the coding regions but may exist in deep intron regions or expression regulatory regions. Deeper insight is needed to interpret the biological significance of mutations in these regions. In this study, we utilized *in silico* analysis tools to pick up a variant in the deep intron region that causes splice abnormalities.

Recently, Wen *et al*. reported 2 cases of DBAS in which WGS was initially negative, but further analysis had revealed a splice mutation at the end of the first non-coding exon of *RPS7* and a deep intronic *de novo* mutation in *RPS19*.[14] In their paper, they also made use of splice prediction tools. They showed that analysis of variants in non-coding regions is useful for the diagnosis and treatment of DBAS, and our current study supports their findings. Meanwhile, they reported that their *RPS19* mutation (NM_001022.4:c.172+350C>T) is a splicing mutation that creates a novel exon in intron 3, resulting in the appearance of a PTC. This is similar to our variant but differs in that their data show that the transcripts containing the novel exon account for 50.9% of the total *RPS19* mRNA, which is considerably more than ours. To investigate the reason for this difference, we analyzed their transcript sequences. Contrary to their interpretation, the c.172+350C>T variant appeared to cause an 81-bp insertion without a PTC, resulting in the in-frame addition of 27 amino acid. We, therefore, consider our transcript with a PTC and their transcript without a PTC as different types. It is important to note that, in the case of a deep intronic variant resulting in PTC, such as in our case, transcripts could be readily degraded by NMD, preventing mutation function analysis.

MO can induce exon skipping by inhibiting mRNA splicing, and has already been applied in studies of neuromuscular diseases such as Duchenne muscular dystrophy.[15] In this study, MO was also effective in suppressing abnormal splicing of *RPS19* mRNA, so it may be possible to use MO in the future to treat DBAS with a splicing abnormality that causes extra exons to appear in the transcripts.

In conclusion, by extending the scope of analysis to deep introns of WGS data, we identified a variant that causes splicing abnormalities in *RPS19* in a case of DBAS. This study demonstrates the importance of analyzing deep intronic regions in the search for mutations causing DBAS when no mutations are detected in coding regions.

Authors

Rika Kanezaki,[1] Tsutomu Toki,[1] Ryo Okuse,[1,2] Akie Kobayashi,[1] Moeka Sato,[1] Sayaka Kimura,[1] Ko Kudo,[1] Tomohiko Sato,[1] Tatsuhiko Tanaka,[1] Kenichi Yoshida,[3] Yosuke Kawai,[4] Katsushi Tokunaga,[4] Junko Takita,[5] Seishi Ogawa,[6-8] Kiminori Terui[1] and Etsuro Ito[1,9]

[1]Department of Pediatrics, Hirosaki University Graduate School of Medicine, Hirosaki; [2]Department of Pediatrics, NHO Hirosaki General Medical Center, Hirosaki; [3]Division of Cancer Evolution, National Cancer Center Research Institute, Tokyo; [4]Genome Medical Science Project, National Institute of Global Health and Medicine, Japan Institute for Health Security, Tokyo; [5]Department of Pediatrics, Graduate School of Medicine, Kyoto University, Kyoto; [6]Department of Pathology and Tumor Biology, Graduate School of Medicine, Kyoto University, Kyoto; [7]Institute for the Advanced Study of Human Biology (ASHBi), Kyoto University, Kyoto; [8]Kindai University Faculty of Medicine, Osaka and [9]Department of Community Medicine, Hirosaki University Graduate School of Medicine, Hirosaki, Japan

Correspondence:
E. ITO - eturou@hirosaki-u.ac.jp

https://doi.org/10.3324/haematol.2025.300131

Received: October 29, 2025.
Accepted: December 30, 2025.
Early view: January 22, 2026.

Disclosures

No conflicts of interest to disclose.

Contributions

RK designed, organized and performed the experiments, analyzed and interpreted the results, and wrote the manuscript; TTo designed and organized the experiments, analyzed and interpreted the results, and helped write the manuscript; RO analyzed and interpreted the results, and helped write the manuscript; AK collected samples, interpreted the results, and helped write the manuscript; MS and SK carried out the experiments; KK, TS, TTa, KY, YK, KTo, JT, SO and KTe analyzed and interpreted the results; EI organized the experiments and wrote the manuscript.

Acknowledgments

The authors would like to thank H. Kudo and Y. Kudo for their technical assistance. We would also like to thank Dr. Atsushi Miyawaki for use of the HUDEP-2 cell line.

Funding

This work was supported by the research grant (Research on Measures for Intractable Disease: 25FC1010) from the Ministry of

Health, Labour and Welfare of Japan and Practical Research Project for Rare/Intractable Disease from Japan Agency for Medical Research and Development (AMED).

Data-sharing statement

The whole-genome sequencing data from this study are available from the corresponding author on reasonable request.

References

1. Wlodarski M, Vlachos A, Farrar J, et al. Diagnosis, treatment, and surveillance of Diamond-Blackfan anaemia syndrome: international consensus statement. Lancet Haematol. 2024;11(5):e368-e382.
2. Ulirsch JC, Verboon JM, Kazerounian S, et al. The genetic landscape of Diamond-Blackfan anemia. Am J Hum Genet. 2018;103(6):930-947.
3. Da Costa L, Leblanc T, Mohandas N. Diamond-Blackfan anemia. Blood. 2020;136(11):1262-1273.
4. Gripp KW, Curry C, Olney AH, et al. Diamond-Blackfan anemia with mandibulofacial dystostosis is heterogeneous, including the novel DBA genes TSR2 and RPS28. Am J Med Genet A. 2014;164A(9):2240-2249.
5. O'Donohue M, Da Costa L, Lezzerini M, et al. HEATR3 variants impair nuclear import of uL18 (RPL5) and drive Diamond-Blackfan anemia. Blood. 2012;122(7):3111-3126.
6. Sankaran V, Ghazvinian R, Do R, et al. Exome sequencing identifies GATA1 mutations resulting in Diamond-Blackfan anemia. J Clin Invest. 2012;122(7):2439-2443.
7. Toki T, Yoshida K, Wang R, et al. De novo mutations activating germline TP53 in an inherited bone-marrow-failure syndrome. Am J Hum Genet. 2018;103(3):440-447.
8. Utsugisawa T, Uchiyama T, Toki T, et al. Erythrocyte glutathione is a novel biomarker of Diamond-Blackfan anemia. Blood Cells Mol Dis. 2016;59:31-36.
9. Barrio A, Eriksson O, Badhai J, et al. Targeted resequencing and analysis of the Diamond-Blackfan Anemia disease locus RPS19. PLos One. 2009;4(7):e6172.
10. Hentze M, Kulozik A. A perfect message: RNA surveillance and nonsense-mediated decay. Cell. 1999;96(3):307-310.
11. Kurita R, Suda N, Sudo K, et al. Establishment of immortalized human erythroid progenitor cell lines able to produce enucleated red blood cells. PLos One. 2013;8(3)e59890.
12. Kanezaki R, Toki T, Terui K, et al. Mechanism of KIT gene regulation by GATA1 lacking the N-terminal domain in Down syndrome-related myeloid disorders. Sci Rep. 2022;12(1):20587.
13. Summerton J. Morpholino, siRNA, and S-DNA compared: impact of structure and mechanism of action on off-target effects and sequence specificity. Curr Top Med Chem. 2007;7(7):651-660.
14. Wen T, Boyden S, Hocutt C, et al. Identification of 2 novel noncoding variants in patients with Diamond-Blackfan anemia syndrome by whole genome sequencing. Blood Adv. 2025;9(10):2443-2452.
15. Clemens P, Rao V, Connolly A, et al. Long-term functional efficacy and safety of viltolarsen in patients with Duchenne muscular dystrophy. J Neuromuscul Dis. 2022;9(4):493-501.